

Original Research

Prospective Registration of Human Head Magnetic Resonance Images for Reproducible Slice Positioning Using Localizer Images

Egbert Gedat, PhD,^{1*} Juergen Braun, PhD,¹ Ingolf Sack, PhD,² and Johannes Bernarding, PhD, MD^{1,2}

Purpose: To facilitate assessing brain tumor growth and progression of stroke lesions by reproducible slice positioning in human head magnetic resonance (MR) images, a method for prospective registration is proposed that adjusts the image slice position without moving the patient and with no additional scans.

Materials and Methods: The gradient reference frame of follow-up examinations was adjusted to achieve the same image slice positioning relative to the patient as in the previous examination. The three-dimensional geometrical transformation parameters for the gradients were determined using two-dimensional image registration of three orthogonal localizer images. The method was developed and evaluated using a phantom with arbitrarily adjustable position. Feasibility for in vivo applications was demonstrated with brain MR imaging (MRI) of healthy volunteers.

Results: Standard retrospective registration was used for assessing the quality of the method. The accuracy of the realignment was $0.0 \text{ mm} \pm 1.2 \text{ mm}$ and $-0.2^\circ \pm 0.9^\circ$ (mean \pm SD) in phantom experiments. In 10 examinations of volunteers, misalignments up to 49.2 mm and 21° were corrected. The accuracy of the realignment after prospective registration was $0.1 \text{ mm} \pm 1.5 \text{ mm}$ and $0.2^\circ \pm 1.5^\circ$.

Conclusion: Image-based prospective registration using localizer images of the pre- and postexaminations is a robust method for reproducible slice positioning.

Key Words: prospective registration; slice positioning; MR imaging; neuroimaging; cross-correlation

J. Magn. Reson. Imaging 2004;20:581–587.
© 2004 Wiley-Liss, Inc.

FOLLOW-UP EXAMINATIONS of cerebral diseases such as stroke or brain tumors require a precise comparison

of changes in unaffected and pathologic tissues (1). Usually, the slices are positioned manually with the use of anatomical landmarks like the intercommissural line. Therefore, additional data have to be acquired in follow-up measurements and visually compared to initial examinations by the physician. Depending on the deviations and the patient's condition, the slices may then be repositioned and images are compared iteratively until sufficient congruence is found. Since this procedure depends on visual estimates and may be very time consuming, an automated algorithm would be of great advantage to both diagnostics and patient handling. To improve diagnostics, especially of small lesions such as Multiple Sclerosis (MS) foci, retrospective registration (2,3) can be used, as it is common in functional magnetic resonance imaging (fMRI) (4). However, these techniques are often compromised by interpolation artifacts (5), in particular at boundaries between different tissue structures.

In MRI, prospective registration can be used to correct for misalignments prior to subsequent measurements without the need for patient repositioning. The corresponding transformation matrix is then used to correct the slice position by adaptation of the gradients. Different approaches for prospective registration have been reported, mainly triggered by the need for real-time motion correction in fMRI. Navigator echoes were developed for imaging moving structures (6,7) and for fMRI (8). The technique was advanced to orbital navigator echoes (9–11) and spherical navigator echoes (12). Image-based methods for prospective motion correction in fMRI were proposed that use typical three-dimensional data sets from fMRI time series (13,14). Recently, a method was introduced that matches localizer images on a three-dimensional statistical atlas of the brain (15).

Interexamination prospective registration for monitoring cerebral diseases requires the development of a method that corrects for larger deviations and potentially altered tissue that might occur after tumor therapy. For clinical applications, the method should be based on fast and robust registration algorithms that use data acquired in the standard clinical settings and that do not rely on information about the underlying pathophysiological processes. Therefore, we chose a prospective registration method that employed the stan-

¹Institutes for Medical Informatics, Charité University Medicine Berlin, Germany.

²Radiology, Charité University Medicine, Berlin, Germany.

Contract grant sponsor: German Research Foundation; Contract grant number: DFG Be 1824/4-1.

This work was presented as a poster at the 12th Annual Meeting of ISMRM, Kyoto, Japan, 2004. Parts of this work were presented as a poster at the 11th Annual Meeting of ISMRM, Toronto, Canada, 2003.

*Address reprint requests to: E.G., Institut für Medizinische Informatik, Charité—Universitätsmedizin Berlin, Hindenburgdamm 30, 12200 Berlin, Germany. E-mail: egbert.gedat@charite.de

Received January 5, 2004; Accepted May 11, 2004.

DOI 10.1002/jmri.20153

Published online in Wiley InterScience (www.interscience.wiley.com).

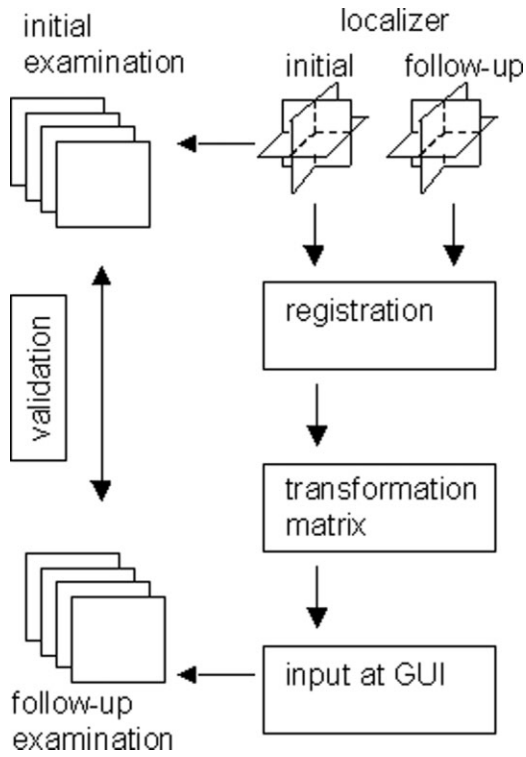


Figure 1. Flowchart of the prospective registration using localizer images.

standard localizers that are acquired in practically all MR examinations.

Although some public-domain image registration tools are available, such as Automated Image Registration (AIR) (16) and Statistical Parametric Mapping (SPM) (17), the hard- and software restrictions of MR scanners necessitated the development of specialized image-based registration procedures. In this study, prospective image registration was attained by cross-correlation (18) of the localizer images. AIR served to evaluate and validate the results of the new method.

In the following, the image-based registration algorithm is derived and demonstrated by phantom experiments and examinations on healthy volunteers.

MATERIALS AND METHODS

The introduced prospective registration procedure consists of the following steps: 1) primary examination with acquisition of the initial localizer and diagnostic image set of the head, 2) follow-up acquisition of localizer images and registration to initial localizer images from the primary measurement, 3) calculation of the transformation matrix and adaptation of the gradient control, and 4) follow-up examination with acquisition of the diagnostic follow-up image set. A schematic representation of the method is displayed in Fig. 1.

Registration

The three orthogonal localizer images of the initial examination were used as reference for the patient position. In the following, these images are labeled I_i , where the index $i = x, y, z$ refers to Cartesian coordinate axes. For standard localizer scans of the head, these axes are aligned with the principal axes of the scanner. Their relation to the anatomic notation is depicted in Fig. 2a–c. Corresponding to I_i , the localizer images of the follow-up examination were denoted as F_i . The images were registered pairwise with respect to the shift vectors s_i and the rotation angles ϕ_i as components of the rotation vector ϕ . The resulting new localizer images $F'_i(\phi_i, s_i)$ represented the patient position corresponding to I_i . The rotation registrations were performed by searching the maximum value $\max(\chi_{\max})$ of the largest element χ_{\max} of the cross-correlation matrix $\chi(F'_i(\phi_i), I_i)$ with respect to ϕ_i :

$$\chi_{\max}(F'_i, I_i) = \max(\chi_{\max}(F_i(\phi_i), I_i)) \quad (1)$$

Rotations of the images were carried out using bilinear interpolation. After rotation registration, the shift vec-

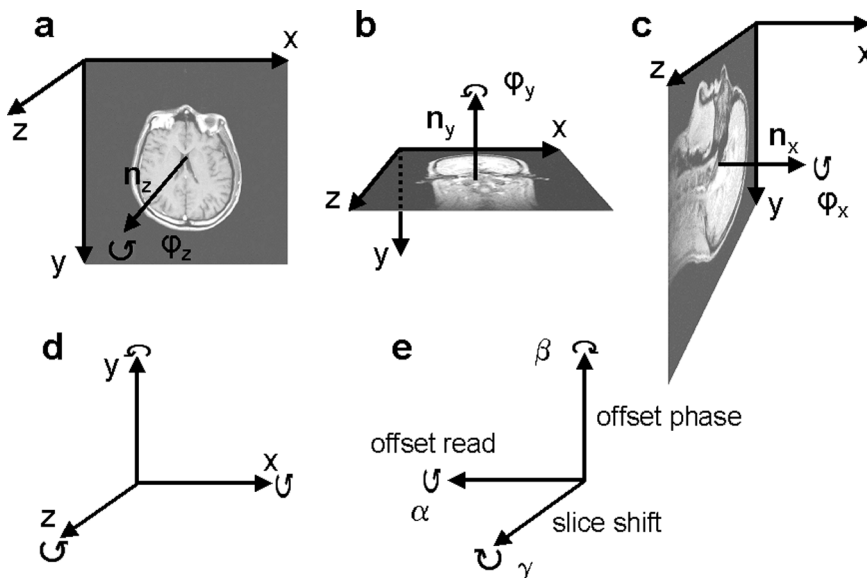


Figure 2. Coordinate systems used in this paper. **a–c:** Image coordinate system for transversal, coronal, and sagittal planes, respectively. $n_{x,y,z}$ denote the rotation axes during image registration. **d:** Principal axis system. **e:** Tomograph coordinate system. The parameters $\alpha, \beta,$ and γ were used for adjusting the gradients. As indicated by arrows, rotations were applied in the positive direction.

tors \mathbf{s}_i were determined by subtracting the positions of the maxima of the cross-correlation $\chi(\mathbf{F}_i, \mathbf{I}_i)$ and the autocorrelation $\chi(\mathbf{I}_i, \mathbf{I}_i)$, respectively:

$$\mathbf{s}_i = \begin{pmatrix} m - p \\ n - q \end{pmatrix}; \xi_{mn} = \chi_{\max}(\mathbf{I}_i, \mathbf{I}_i); \chi_{pq} = \chi_{\max}(\mathbf{F}_i, \mathbf{I}_i) \quad (2)$$

Rotations and translations were oriented as defined in Fig. 2a–c. Then the matrix indices of \mathbf{F}_i were shifted by \mathbf{s}_i , and the registration was iterated using $\mathbf{F}_i(\phi_i, \mathbf{s}_i)$ as the starting point for achieving a successive refinement of the parameter grid. The rotation angles ϕ_i were varied in three iteration steps within $\pm 40^\circ$, $\pm 5^\circ$, and $\pm 1^\circ$. At the end of the procedure, the final angles ϕ_i were achieved as the sum over the correction angles of the three iterations. The final shift vectors \mathbf{s}_i were calculated again by Eq. [2] using the final rotation angles. Each shift vector $\mathbf{s}_i = [s_{i,1}, s_{i,2}]$ comprised a two-element vector, which was used to calculate the three-dimensional shift vector in the image coordinate system:

$$\mathbf{s}_{3D} = \left(\frac{s_{z,1} + s_{y,1}}{2}, \frac{s_{z,2} + s_{x,2}}{2}, \frac{s_{y,2} + s_{x,1}}{2} \right) \quad (3)$$

This allowed, together with ϕ_i , correction for the translation and rotation of MR images in three dimensions. The algorithm was implemented in MATLAB (MathWorks, Inc., Natick, MA). The computation time on a Pentium 4, 1.6-GHz computer was 45 seconds.

Calculation and Adjustment of the Updated Gradient Reference Frame

The tomograph gradients were adapted using the shift vector \mathbf{s}_{3D} (Eq. [3]) and the Euler angles (α, β, γ) derived from ϕ . The angles ϕ_i were regarded as the Cartesian components of a three-dimensional rotation by the angle $\phi = |\phi|$ around an axis $\mathbf{n} = \phi/\phi$ (11). This rotation, $\mathbf{R}_n(\phi)$, was related to the Euler angles according to:

$$\mathbf{R}_n(\phi) = \mathbf{R}_z(\gamma)\mathbf{R}_y(\beta)\mathbf{R}_x(\alpha). \quad (4)$$

$\mathbf{R}_{x,y,z}$ describe the common rotation matrices for counterclockwise rotation around the x -, y -, and z -axes, respectively.

The rotation angles α and β were changed manually using the positioning interface of the tomograph's operating system. To achieve an in-plane rotation of the field of view (FOV), the pulse sequence had to be changed so that the gradient reference frame was rotated with γ around the new z -axis. Therefore, the amplitudes of the gradients in the readout and phase-encode directions were recalculated and adapted in the MR sequence. To reduce the examination time, 61 sequences with varying γ in the interval $-30^\circ \leq \gamma \leq 30^\circ$ in 1° increments were implemented and precompiled, because the scanner did not allow changing this parameter interactively.

To account for the nonprincipal coordinate system of the scanner (see Fig. 2), the shift vector \mathbf{s}_{3D} in Eq. [3]

and the rotation axis \mathbf{n} in Eq. [4] were transformed into the tomograph coordinate system.

Experiments

All studies were performed on a Siemens Vision 1.5-T MR scanner (Siemens, Erlangen, Germany) equipped with a Numaris 3.3b operating system. A similar protocol was applied for phantom and volunteer studies. An initial set of localizer images (FOV = 200 mm (phantom) and 300 mm (volunteer), slice thickness = 8 mm, TR = 15 msec, TE = 6 msec, matrix = 256×256) in the transversal, coronal, and sagittal orientations, together with 13 T_1 -weighted images (FOV = 200 mm (phantom) and 300 mm (volunteer), slice thickness = 5 mm, slice distance = 1 mm, TR = 300 msec, TE = 12 msec, matrix = 256×256) in the transversal orientation, were recorded. After changing the object's position, follow-up localizer images were recorded. All localizer data were acquired without changing the gradient frame to ensure the alignment of the gradient axes with the tomograph coordinate system. After data acquisition, the localizer data were transferred to an external PC (Pentium 4, 1.6 GHz) and the registration was performed as described above. The new settings were entered at the tomograph console followed by the acquisition of the new images.

Accuracy and duration of the method were tested with an agarose gel phantom, which was mounted on a carrier that could be moved and adjusted in all six degrees of freedom of rigid-body motion. In each experiment, the position of the phantom was varied with respect to all six parameters. In 12 experiments, 12 different, arbitrary combinations of the displacements and rotations, with $x = \pm 10$ mm, $y = \pm 5$ mm, $z = \pm 10$ mm, and $\phi_i = \pm 10^\circ$ relative to the initial position of the phantom, were applied.

The new prospective registration method was evaluated performing 10 in vivo studies with three volunteers. Informed consent was obtained from each volunteer after the nature of the procedure had been fully explained. Between pre- and postscans, the volunteers were asked to rotate their heads and to move within the magnet. Rotations were restricted to $\pm 30^\circ$, and the head should not be moved out of the coil. The follow-up images were recorded with an initial slice shift of -70 mm (volunteers 1 and 3) and -40 mm (volunteer 2) to image the brain. The maximum time between the follow-up localizer and the start of the follow-up examination was 4.8 minutes.

Validation of the Results

To specify the accuracy of the registration, the follow-up T_1 -weighted image sets were retrospectively registered to the initial images using a three-dimensional rigid-body model within AIR 5.2.2 (16). In phantom experiments, the accuracy of the method was additionally assessed by comparing the results of the registration with the real object displacement, which was defined by the settings of the carrier unit. Since the image rotation axes in the registration procedure were fixed in the center of the images, these axes were not necessar-

Table 1
Results of Phantom Experiments*

N=12	Δx / mm		Δy / mm		Δz / mm		$\Delta\phi_x$ / °		$\Delta\phi_y$ / °		$\Delta\phi_z$ / °	
	geo	AIR	geo	AIR	geo	AIR	geo	AIR	geo	AIR	geo	AIR
1	-0.7	0.7	-1.2	0.2	2.6	0.0	0.8	0.4	0.3	2.0	1.0	0.4
2	0.6	0.7	-0.1	-1.9	4.6	0.3	1.2	0.1	-0.2	1.9	0.1	-0.4
3	-0.2	1.1	-0.1	-1.2	1.2	-1.8	2.4	-0.1	0.7	0.1	-0.4	0.7
4	-1.6	1.4	-0.1	-0.3	-1.7	-0.4	-0.6	-1.5	-0.6	-1.8	0.4	-0.7
5	1.8	1.4	1.5	-1.4	-2.3	-0.1	0.2	-0.1	-0.5	-1.8	1.0	0.0
6	2.2	-1.0	0.5	0.6	-1.1	-2.9	3.0	0.6	-1.2	0.1	2.0	-0.3
7	1.2	1.4	-1.0	-0.5	-0.4	2.6	-1.0	0.0	-0.5	0.0	-1.4	0.1
8	-1.2	-0.3	0.6	-1.3	-0.2	2.8	-1.0	0.5	-0.5	-0.8	-1.4	-0.9
9	-0.3	-0.5	0.8	0.6	-0.5	0.7	1.4	0.1	-0.5	-1.5	-1.3	0.0
10	1.6	-1.0	0.2	-0.8	0.1	0.2	-2.4	-1.9	0.5	-0.5	-1.2	-0.3
11	-2.0	-0.1	0.3	-0.5	0.4	0.0	-2.4	-0.3	0.7	-1.9	-2.4	-1.0
12	-2.7	-0.1	1.2	0.6	0.5	-0.9	-0.8	-1.4	0.3	1.0	-2.3	-0.0
mean	-0.1	0.3	0.2	-0.5	0.3	0.0	0.1	-0.3	-0.1	-0.3	-0.5	-0.2
SD	1.6	0.9	0.8	0.9	1.9	1.6	1.7	0.8	0.6	1.4	1.4	0.5

*Difference between results obtained with prospective registration and (geo) true geometric values including apparent translations and (AIR) calculated values and results of the retrospective three-dimensional registration with AIR.

geo = geometrical comparison, AIR = registration with AIR, SD = standard deviation.

ily aligned with the physical rotation axes of the phantom. The latter are located at a point in the images that is defined by the position of the carrier in the magnet. The line between these two points produces an artificial translation of the phantom when the images are rotated around the center. This so-called apparent translation (11) had to be included for achieving comparability between the position parameters of the carrier unit and the registration results.

RESULTS

Adjustable Phantom Study

For the phantom studies, both the geometric data of the object position compared to the results of the new prospective registration method and the results of the retrospective three-dimensional registration are listed (see Table 1). The number of the given registration parameters corresponds to the degrees of freedom within the ϕ and s_{3D} transformations. For assessing the accuracy of the method, the averaged transformations $\bar{\phi}$ and \bar{s}_{3D} were calculated. Using these terms, the accuracy of the prospective registration relative to the position of the phantom carrier was determined with (mean \pm SD) $\Delta\bar{\phi} = -0.2^\circ \pm 1.3^\circ$ and $\Delta\bar{s}_{3D} = 0.1 \text{ mm} \pm 1.5 \text{ mm}$. Using retrospective registration as the standard method, $\Delta\bar{\phi} = -0.2^\circ \pm 0.9^\circ$ and $\Delta\bar{s}_{3D} = 0.0 \text{ mm} \pm 1.2 \text{ mm}$ were found.

Volunteer Study

The image-based prospective registration algorithm corrected misalignments of the elements of the translation vectors s_{3D} that varied from -8.8 to 49.2 mm (x -direction), -1.8 to 18.2 mm (y -direction), and -37.5 to 23.4 mm (z -direction). Rotations ranged between $-8.6^\circ \leq \phi_x \leq 16.5^\circ$, $-11.1^\circ \leq \phi_y \leq 3.2^\circ$, and $-22.0^\circ \leq \phi_z \leq 19.5^\circ$. An example of the image-based registration of localizer images is shown in Fig. 3.

The geometric correction parameters of all 10 in vivo registrations are displayed in Table 2 together with the remaining misalignment of the position after prospec-

tive registration. The error of all in vivo registrations was found with $\Delta\bar{\phi} = 0.2^\circ \pm 1.5^\circ$ and $\Delta\bar{s}_{3D} = 0.1 \text{ mm} \pm 1.5 \text{ mm}$ (mean \pm SD). An example of prospective in vivo registration is shown in Fig. 4. For comparison, the initial data (first row) are displayed together with the unaligned images as they would appear in the follow-up examination, without prospective registration (second row), and the corresponding images after applying the new prospective registration method (third row). For demonstration, only every second slice of a 13-slice series of a study of a volunteer is shown.

DISCUSSION

It was demonstrated that prospective registration of MR examinations could be achieved using standard orthogonal localizer images. If such localizer prescans are stored together with the diagnostic image data, it is possible to adjust the gradient frame of follow-up examinations. This allows the alignment of the current slice positions to those of former studies. Since no additional acquisitions are required to compensate for different patient positions, the introduced method is feasible for all longitudinal examinations, where the comparability of two-dimensional MR image slices is a prerequisite for successful diagnosis. The method is easy to implement on conventional tomographs and easy to incorporate into standard clinical MR applications. As demonstrated even on tomographs with restricted software capabilities, prospective registration based on localizer images can be implemented. However, in this case some tradeoffs in process time and accuracy have to be taken into account. In the current implementation, the additional effort for off-line computation was the most time consuming step. Nevertheless, the overall procedure, starting from the upload of the reference localizer image data until the adjustment of the gradient control, could be accomplished within five minutes. Such delay between the examinations was assessed by physicians of our hospital as a reasonable

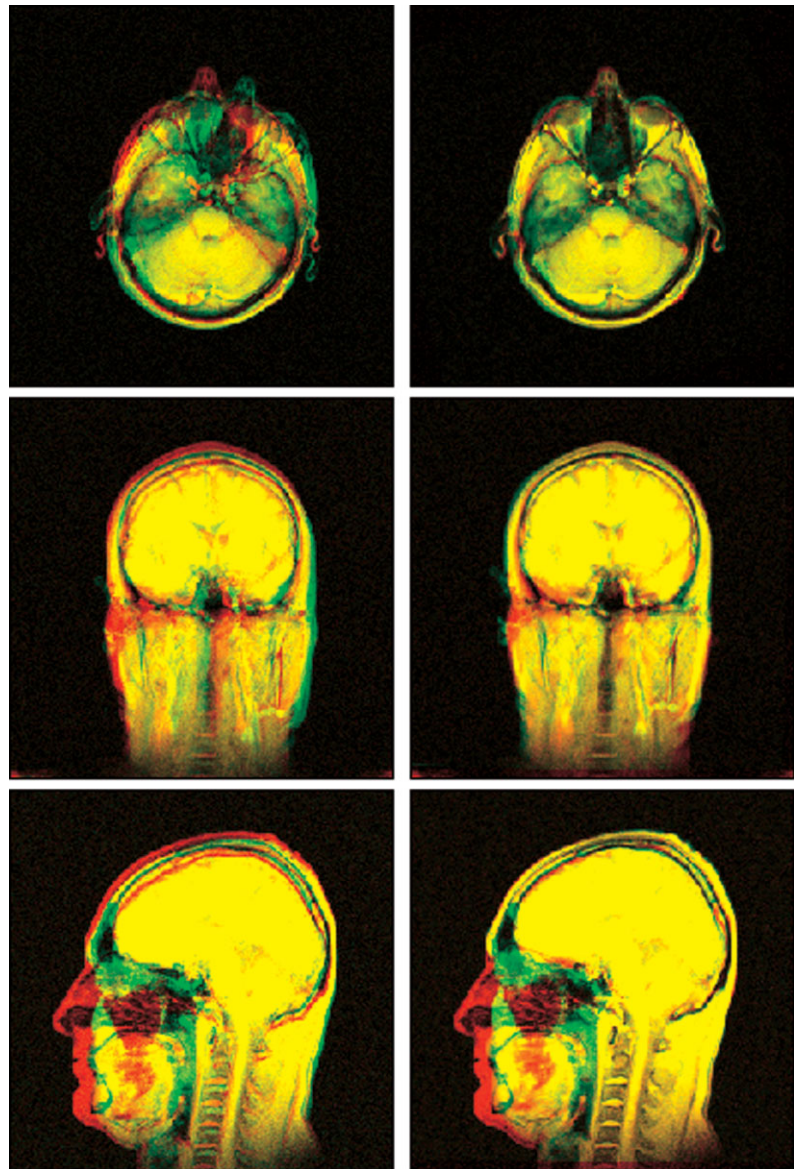


Figure 3. Localizer images before (left column) and after (right column) calculation of the registration (experiment 1 in Table 2). From top to bottom: Transversal, coronal, and sagittal slices. The initial localizers are red and the follow-up localizers are green. Yellow pixels are red and green. The sagittal images are an example for good registration results, although markedly different slices were acquired in the initial and follow-up localizers.

compromise for gaining the advantage of identical slice positions between the examinations.

To appreciate the accuracy of the localizer-based registration, the resolution for translation and rotation of the images can be distinguished. Both image transformations result in a systematic error, which is due to the pixel-based definition of the image transformation, i.e., $\Delta s_p = \pm 0.5$ pixel for translations and $\Delta \phi_p = \pm \arctan(1/\text{matrix size})$ for rotations, respectively. For the use of the geometrical position of the phantom, systematic errors due to tolerances in the adjustment of the carrier were found with $\Delta s_a = \pm 0.5$ mm for translations and $\Delta \phi_a = \pm 0.5^\circ$ for rotations. Using retrospective registration as the standard, a systematic error of $\Delta \phi_g = \pm 0.5^\circ$ for rotations must be considered, which stems from the 1° grid of the angle adjustments. Thus, for the phantom studies the total systematic error for geometric comparison $\Delta s = \pm 0.9$ mm and $\Delta \phi = \pm 0.7^\circ$ and $\Delta s = \pm 0.4$ mm and $\Delta \phi = \pm 0.7^\circ$ for retrospective validation, respectively.

The accuracy achieved in the volunteer studies was close to that of the phantom experiments. Due to the

larger FOV, the pixel-based systematic error was increased from $\Delta s_p = \pm 0.4$ mm to ± 0.6 mm. The total systematic error for retrospective validation of the volunteer data was then $\Delta s = \pm 0.6$ mm and $\Delta \phi = \pm 0.7^\circ$. However, possible patient motion during the examinations would exceed the systematic errors mentioned above. Therefore, the in vivo tolerances of $\Delta \bar{s}_{3D} = \pm 1.5$ mm and $\Delta \bar{\phi} = \pm 1.5^\circ$ were mainly attributed to motion.

Comparison of the accuracy achieved by the new prospective registration method to literature values of varying registration techniques is hampered by different restrictions of the allowed motion. Restricted to in-plane motion, an SD of 0.054 pixels and 0.17° was reported (19). Using a technique of orbital navigator echoes, inaccuracies partly greater than 1 mm and 1.5° with restricted motions in the range of $\pm 8^\circ$ and ± 8 mm (11) were found. In contrast, for the presented experiments, displacements up to 49.2 mm and 21° were allowed. Thus, the accuracy of the method proposed here is comparable to the accuracy of the orbital navi-

Table 2
Results of Volunteer Studies*

Subject	No.	Δx / mm	Δy / mm	Δz / mm	$\Delta\varphi_x$ / °	$\Delta\varphi_y$ / °	$\Delta\varphi_z$ / °
1	1	-1.7 (-5.9)	1.1 (0.0)	0.5 (6.4)	-0.2 (1)	-0.2 (-1)	-1.1 (15)
1	2	-0.6 (0.6)	2.9 (10.5)	0.0 (-18.2)	1.3 (-17)	0.7 (-1)	-0.5 (-2)
1	3	-1.2 (10.0)	-3.9 (7.6)	-0.8 (-37.5)	-1.3 (-3)	0.4 (0)	-2.0 (-20)
2	4	-0.7 (-8.8)	-0.4 (1.8)	-0.2 (8.2)	-0.3 (1)	0.3 (3)	0.0 (14)
2	5	0.1 (-4.7)	0.0 (0.0)	0.2 (0.0)	0.0 (-4)	0.0 (0)	0.2 (4)
2	6	-1.4 (-8.8)	0.1 (0.6)	0.2 (-5.3)	-0.6 (7)	-0.2 (4)	-1.0 (15)
3	7	-2.1 (-8.2)	0.2 (0.6)	-2.3 (23.4)	-1.2 (2)	2.7 (-5)	-1.2 (20)
3	8	1.0 (-0.6)	1.9 (-1.8)	0.2 (19.9)	0.9 (-15)	0.1 (0)	-0.3 (-1)
3	9	0.2 (40.4)	2.2 (18.2)	0.8 (4.1)	1.8 (6)	-1.0 (-12)	0.9 (-21)
3	10	1.4 (49.2)	0.9 (13.5)	2.8 (10.5)	5.6 (1)	2.3 (-2)	0.7 (-1)
Mean		-0.5	0.5	0.1	0.3	0.5	-0.4
SD		1.2	1.9	1.3	2.2	1.1	0.9

*Remaining deviations after prospective registration determined with three-dimensional retrospective registration (AIR). Absolute correction parameters, i.e., the elements of s_{3D} and α , β , γ , are listed in brackets. SD = standard deviation.

gator echo technique. Significantly larger displacements are not expected for clinical examinations.

Surveying the volunteer studies, two entries of Table 2 need further comment: the deviation of -3.9 mm in the y -direction of experiment 3 and the deviation of 5.6° for rotation around the x -axis in experiment 10. In the first case, the step of registration was accomplished with high accuracy. However, the rather large displacement of the volunteer in the z -direction shifted the axial slice of the follow-up localizer to a new anatomical position. Here, the cross section of the head was shifted upward due to its shape and not due to motion. This was misinterpreted by the algorithm as a shift in the y -direction. In the second case, the large displacement of the volunteer in the x -direction shifted the sagittal follow-up localizer to the lateral edge of the brain. Here, the diameter of the head was markedly smaller and anatomic structures were no longer similar to those on the initial image. For

future applications of the prospective registration using localizer images, those situations must be avoided by a repetition of the registration after the patient has been repositioned.

The success of the technique might be surprising considering the information content of the localizer images. But, as outlined above, any rotation can be represented by projections of its rotation axis on three orthogonal planes. The accurate reconstruction of these projections from the localizer scans surely depends on the shape and structure of the object; i.e., a uniform sphere will always produce zero degree rotations in the registration. In contrast, the approximately ellipsoid shape of the head, together with the intensity distribution in the localizer scans due to skin, skull, and brain, appears to support the application of the cross-correlation method.

In conclusion, the prospective registration using localizer images was successfully tested on phantoms

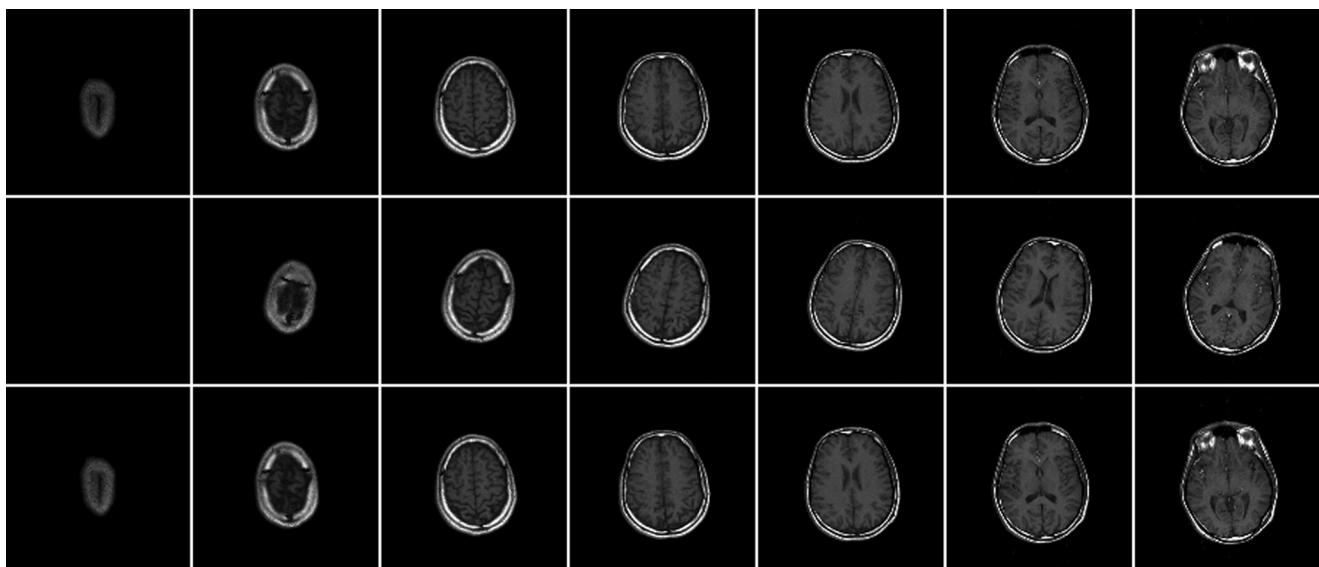


Figure 4. T_1 -weighted image sets of one volunteer (experiment 4 in Table 2). Top row: Initial examination. Middle row: Follow-up examination after motion of the head without prospective registration. Bottom row: Follow-up examination after prospective registration. Every second image slice of the data is shown.

and healthy volunteers. Realigned and referenced images matched well and with good accuracy. Compared to a full rigid-body three-dimensional registration, the procedure was very time efficient since the registration could be accomplished using only three two-dimensional images. No additional data had to be acquired prior to the examination. Since patient motion cannot be excluded during registration and examination, an additional real-time motion correction would ensure identical slice positions.

ACKNOWLEDGMENTS

The authors thank R. Woods for support with AIR and Ms. Jean Pietrowicz for carefully proofreading the manuscript.

REFERENCES

- Bernarding J, Braun J, Hohmann J, et al. Histogram-based characterization of healthy and ischemic brain tissues using multiparametric MR imaging including apparent diffusion coefficient maps and relaxometry. *Magn Reson Med* 2000;43:52–61.
- West J, Fitzpatrick JM, Wang MY, et al. Comparison and evaluation of retrospective intermodality brain image registration techniques. *J Comput Assist Tomogr* 1997;21:554–566.
- Maintz JBA, Viergever MA. A survey of medical image registration. *Med Image Anal* 1998;2:1–36.
- Friston KJ, Williams S, Howard R, Frackowiak RSJ, Turner R. Movement-related effects in fMRI time-series. *Magn Reson Med* 1996;35:346–355.
- Ostuni JL, Santha AKS, Matta VS, et al. Analysis of interpolation effects in the reslicing of functional MR images. *J Comput Assist Tomogr* 1997;21:803–810.
- Ehman RL, Felmlee JP. Adaptive technique for high-definition MR imaging of moving structures. *Radiology* 1989;173:255–263.
- McGee KP, Felmlee JP, Manduca A, Riederer SJ, Ehman RL. Rapid autocorrection using prescan navigator echoes. *Magn Reson Med* 2000;43:583–588.
- Lee CC, Jack Jr CR, Grimm RC, et al. Real-time adaptive motion correction in functional MRI. *Magn Reson Med* 1996;36:436–444.
- Fu ZW, Wang Y, Grimm RC, et al. Orbital navigator echoes for motion measurements in magnetic resonance imaging. *Magn Reson Med* 1995;34:746–753.
- Lee CC, Grimm RC, Manduca A, et al. A prospective approach to correct for inter-image head rotation in fMRI. *Magn Reson Med* 1998;39:234–243.
- Ward HA, Riederer SJ, Grimm RC, Ehman RL, Felmlee JP, Jack Jr CR. Prospective multiaxial motion correction for fMRI. *Magn Reson Med* 2000;43:459–469.
- Welch EB, Manduca A, Grimm RC, Ward HA, Jack Jr CR. Spherical navigator echoes for full 3D rigid body motion measurement in MRI. *Magn Reson Med* 2002;47:32–41.
- Mathiak K, Posse S. Evaluation of motion and realignment for functional magnetic resonance imaging in real time. *Magn Reson Med* 2001;45:167–171.
- Thesen S, Heid O, Mueller E, Schad LR. Prospective acquisition correction for head motion with image-based tracking for real-time fMRI. *Magn Reson Med* 2000;44:457–465.
- van der Kouwe A, Gicquel S, Chen GN, et al. On-line automatic slice positioning and between-scan correction for brain MR protocols. In: *Proceedings of the 11th Annual Meeting of ISMRM, Toronto, Canada, 2003*. p 797.
- Woods RP, Cherry SR, Mazziotta JC. Rapid automated algorithm for aligning and reslicing PET images. *J Comput Assist Tomogr* 1992;16:620–633.
- Friston KJ, Ashburner J, Frith CD, Poline JB, Heather JD, Frackowiak RSJ. Spatial registration and normalization of images. *Human Brain Mapping* 1995;3:165–189.
- Barnea DI, Silverman HF. A class of algorithms for fast digital image registration. *IEEE Trans Comput* 1972;21:179–186.
- Maas LC, Frederick BdB, Renshaw PF. Decoupled automated rotational and translational registration for functional MRI time series data: the DART registration algorithm. *Magn Reson Med* 1997;37:131–139.